Inter-Research Science Publisher

Marine Ecology Progress Series
Volume 752:35–50

Published January 16, 2025
https://doi.org/10.3354/meps14753

Characteristics of autumn phytoplankton communities in the Chukchi Sea: resuspension of settled diatoms to the surface during strong wind events

Yuri Fukai[1,2,4,*], Amane Fujiwara[1], Shigeto Nishino[1], Satoshi Kimura[1], Motoyo Itoh[1], Koji Suzuki[3]

[1]Research Institute for Global Change, Japan Agency for Marine-Earth Science and Technology (JAMSTEC), Yokosuka, Kanagawa 237-0061, Japan

[2]Graduate School of Environmental Science, Hokkaido University, Sapporo, Hokkaido 060-0810, Japan

[3]Faculty of Environmental Earth Science, Hokkaido University, Sapporo, Hokkaido 060-0810, Japan

[4]*Present address:* WPI-Advanced Institute for Marine Ecosystem Change (AIMEC), Tohoku University & JAMSTEC, Yokohama, Kanagawa 236-0001, Japan

ABSTRACT: Phenological changes in microalgal production and community structure are occurring in the Arctic Ocean. In particular, delayed sea ice formation in autumn can extend the microalgal growth season; however, the succession of phytoplankton communities during this longer photoavailable season is poorly understood. Our objective was to relate oceanographic conditions to the variability in total phytoplankton biomass by examining diatom assemblages in the Chukchi Sea during autumn. We combined scanning electron microscopy (SEM) and DNA metabarcoding techniques to characterize diatom communities, including resting spores of the genus *Chaetoceros*. The upper layer from the shelf slope to the basin is generally well stratified and influenced by sea-ice meltwater. This stratification prevents the supply of nutrients from the lower layers; therefore, the diatom community is characterized by the typical autumn diatom genus *Proboscia* near the surface. On the southern shelf, the wind modulates the bottom current, and in turn the current induces the resuspension of sediments and microalgae. Therefore, we speculate that strong winds enhance the currents within the benthic boundary layer, which entrains *Chaetoceros* resting spore-rich sediments and nutrients (including NH_4) to the ocean interior, resulting in a seeding potential for autumn phytoplankton blooms. Multiple data from the cruise and the moorings suggest that the resuspension of sediments and microalgae could commonly occur in the shelf during autumn. The enhanced wind activity in the shallow Chukchi Sea could be important for biogeochemical processes by facilitating the supply of nutrients and viable diatoms from the seafloor to the upper water column.

KEY WORDS: Chukchi Sea · Phytoplankton · Diatom resting spores · Autumn bloom · DNA metabarcoding · Scanning electron microscopy · SEM

1. INTRODUCTION

The Pacific sector of the Arctic consists of a broad, shallow shelf in the Chukchi Sea, and it is recognized as one of the most productive regions in the Arctic during the spring and summer seasons (Springer et al. 1996, Hill et al. 2018). Diatoms play a fundamental role in primary production (e.g. Sergeeva et al. 2010, Giesbrecht et al. 2019, Suzuki et al. 2021) and in the sinking flux of particulate organic carbon (POC) in this area (Lalande et al. 2020). In the Chukchi Sea, especially in the shelf region, diatoms are usually pre-

*Corresponding author: fukaiy@jamstec.go.jp

Publisher: Inter-Research · www.int-res.com

dominant not only during the spring and summer bloom seasons but also from September to October, as indicated by microscopy analyses (Matsuno et al. 2014) and chemotaxonomic algal pigments (Fujiwara et al. 2014). However, autumn phytoplankton communities in the Pacific Arctic have received comparatively less attention than their spring and summer counterparts. There is a need to better understand the algal communities, especially diatoms, during the autumn season.

Diatoms have been conventionally investigated via microscopy due to their large cell size (~5 µm up to 2 mm; Hoppenrath et al. 2009) and various frustule morphologies. This method identifies diatom life stages based on their morphological features. Diatom resting spores form in response to nutrient depletion (Hargraves & French 1983, McQuoid & Hobson 1996) and exhibit morphological features distinct from those of vegetative cells. From an ecological standpoint, diatom resting spores in sediments can lead to a genetically diverse microalgal population (Sundqvist et al. 2018). In addition, the carbon and silicate contents in diatoms are generally higher than those in vegetative cells (Kuwata et al. 1993); thus, diatom resting spores play a critical role in the ocean carbon and silica cycles by sinking to the seafloor (e.g. Rynearson et al. 2013). The differentiation of diatom spores from vegetative cells holds significance from both biogeochemical and ecological perspectives. Nonetheless, microscopy analysis is a time-consuming process that requires a high level of expertise in identifying diatoms at the genus or species level.

A molecular approach, which can mitigate these difficulties in microscopy analysis, has emerged as a recent method for exploring the diversity of eukaryotic organisms, including microalgae. Among the molecular approaches, the use of metabarcoding has notably increased, particularly in aquatic ecosystems (Lopes dos Santos et al. 2022). The metabarcoding technique involves the amplification of a marker gene followed by sequencing of the amplicon. Although several marker genes have been suggested, the 18S rRNA gene is the most common gene used in eukaryotic plankton studies (Lopes dos Santos et al. 2022). The DNA metabarcoding technique allows us to estimate the relative abundance of each algal group based on nucleic acid databases. Since reference databases for sequence annotation are vital and sometimes significantly change the final outputs, reliable databases for protists (i.e. eukaryotic microorganisms), such as the Protist Ribosomal Reference (PR^2) database, have been developed (Guillou et al. 2013). This technique cannot determine diatom size or life stage, so there is a need to compare the 2 analytical methods (i.e. microscopy and DNA metabarcoding techniques). This comparison examines diatom communities while maintaining the validity of previous microscopy studies. However, few studies have compared microscopy and DNA metabarcoding technique data in the Arctic Ocean (Balzano et al. 2017, Gérikas Ribeiro et al. 2020, Šupraha et al. 2022). Furthermore, to our knowledge, this comparison has not been performed in the Chukchi Sea.

In recent years, across much of the Arctic, including the Pacific Arctic, there has been an increase in stormy conditions in open waters from September to October due to delayed sea-ice formation (Ardyna et al. 2014). As a result, fall microalgal blooms have become more common (Ardyna et al. 2014). Strong wind events during autumn over the Chukchi Sea can supply nutrients to the surface, leading to enhanced primary production and microalgal biomass, particularly by large phytoplankton such as diatoms (Nishino et al. 2015). Furthermore, certain diatoms, such as *Dactyliosolen fragilissimus*, *Rhizosolenia* spp., *Cylindrotheca closterium*, *Navicula* spp., and resting spores of *Chaetoceros furcellatus*, have been shown to increase significantly in abundance following such wind events (Yokoi et al. 2016).

While environmental changes during autumn in the Chukchi Sea are known to influence the phenology of microalgal community dynamics, the specific underlying mechanisms remain unclear. In this context, we characterized diatom communities and oceanographic features in the Chukchi Sea during late autumn using scanning electron microscopy (SEM) and DNA metabarcoding techniques.

2. MATERIALS AND METHODS

2.1. Sampling, environmental parameters, and phytoplankton parameters

Our data consist of vertical profiles from 19 stations (bottom depth: 39–1983 m) in the Pacific Arctic region (Fig. 1; Table S1 in the Supplement at www.int-res.com/articles/suppl/m752p035_supp.pdf) collected from 8 to 21 October 2020, during the MR20-05C expedition of RV 'Mirai' (Japan Agency for Marine-Earth Science and Technology). Temperature and salinity were measured using a CTD profiling system (SBE9plus CTD system, Sea-Bird Electronics). Beam transmission was measured by a C-Star transmissometer (WET Labs) attached to the CTD system. The data from the first 5 m layer were used as represen-

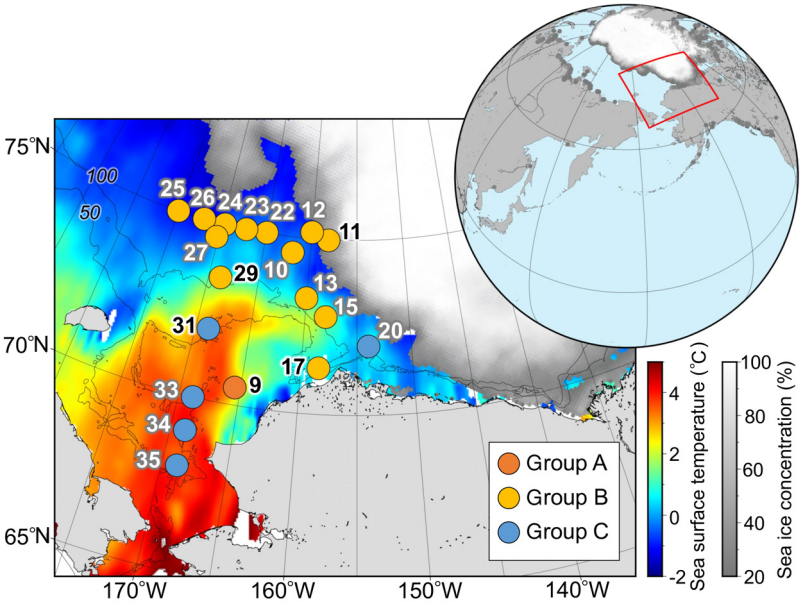

Fig. 1. Water sampling stations in the Chukchi Sea. The colored and grayscale contours indicate the mean sea surface temperature and the mean sea ice concentrations during the sampling period, respectively. The colors at each station denote diatom community groups classified by cluster analysis, and the same group was found in both surface and subsurface layers. Note that Stn 35 was the mooring station

tative values for the surface layer. In the absence of 5 m data, the data from the shallowest depth were assigned as the surface layer.

The fractions of sea-ice meltwater and other freshwater inputs (precipitation, river runoff, and fresh water spread across the surface of the Pacific Arctic) were inferred from salinity and total alkalinity data (Yamamoto-Kawai et al. 2005). The optimum end-member values used for the calculation are outlined by Nishino et al. (2016). We assessed the stratification of the water column through an index proposed as potential energy relative to the mixed state, following Ueno et al. (2020).

For the vertical profiles of chlorophyll *a* (chl *a*) concentration, water samples were collected from 7–13 layers and measured using a fluorometer. Approximately 250 ml of seawater were filtered through ADVANTEC GF-75 filters (nominal pore size 0.3 µm) under gentle vacuum (<0.02 MPa), and the chl *a* was immediately extracted with *N*,*N*-dimethylformamide (DMF) at −20°C for 24 h. In cases where there was a delay before analysis, the filters were immediately stored at −80°C until extraction. After the extraction, chl *a* concentrations were quantified by a fluorometer (10-AU, Turner Designs) calibrated using pure chl *a* (Sigma-Aldrich).

Seawater samples for nutrient, phytoplankton pigment, SEM, and DNA metabarcoding analyses were collected from both the surface and subsurface chl *a* maximum (SCM) layers using a bucket and a Niskin water sampler (Table S1). Although the SCM layers were identified based on the vertical profiles of chl *a* fluorescence, at certain stations without a distinct SCM, samples were obtained from an arbitrary subsurface layer (ASL). Henceforth, the SCM and ASL are referred to as the subsurface layer (SSL).

For nutrient analysis, nitrate, nitrite, ammonium, phosphate, and silicic acid were measured onboard using colorimetric methods with a QuAAtro 2-HR system (BL-Tec) evaluated with certified reference materials (KANSO, lot symbols of CE, CL, CO, and CG). The wind speed throughout the cruise was computed from the ERA5 hourly *u*- and *v*-wind components (Hersbach et al. 2023), with values extracted from the data set close to each sampling site. Current speed data were acquired by a hull-mounted acoustic Doppler current profiler (ADCP) operating at 76.8 kHz (Teledyne RD Instruments) with 8 m depth resolution along the cruise track. We did not separately consider the tidal current effect, but note that Fang et al. (2022) reported the dominance of wind-generated near-inertial energy during the season without ice cover in the Chukchi Sea with shallow depth. Sea surface photosynthetically active radiation (PAR) was continuously monitored using a PAR sensor (PUV-510, Biospherical Instruments) throughout the cruise. Detailed information on the observation and the analytical methods for these basic parameters can be found in Nishino (2020).

2.2. Phytoplankton pigments for chemotaxonomic communities

We collected 1200 ml of seawater from the surface layer and SSL to filter through Whatman GF/F filters (nominal pore size 0.7 µm) under a gentle vacuum (<0.013 MPa), and the filters were immediately frozen in the deep freezer at −80°C onboard. In the shore-based laboratory, we extracted phytoplankton pigments using the DMF bead-beating technique and analyzed them via ultra-high performance liquid chromatography (UHPLC Nexera X2, Shimazu) following the method outlined by Suzuki et al. (2015). The chl *a* biomass of phytoplankton groups was estimated by a pig-

ment-based chemotaxonomic tool using the R software package 'phytoclass' version 1.0.0 (Hayward et al. 2023). In the analysis, we set an iteration length of 500 and a step of 0.009, according to Hayward et al. (2023). We estimated the chl *a* biomass of 8 phytoplankton groups (diatoms, dinoflagellates, prymnesiophytes [haptophytes], chlorophytes, prasinophytes sensu lato, cryptophytes, and cyanobacteria) from 11 pigments (peridinin, 19'-butanoyloxyfucoxanthin, fucoxanthin, 19'-hexanoyloxyfucoxanthin, neoxanthin, prasinoxanthin, violaxanthin, alloxanthin, lutein, zeaxanthin, and chl *b*) following a previous study in the Chukchi Sea (Zhuang et al. 2016). The minimum and maximum values of each pigment:chl *a* ratio for the estimation were obtained by multiplying the pigment ratios in Zhuang et al. (2016) by 0.1 and 3, respectively.

2.3. SEM for diatom communities

We collected 107–120 ml of seawater from the surface layer and SSL into dark bottles for fixation with 10% paraformaldehyde at a final concentration of ca. 0.2%, and the fixed samples were stored at 4°C until further analysis. For the SEM analyses in the shore-based laboratory, 5–61 ml of the fixed seawater were filtered through polycarbonate filters (pore size 2.0 µm; Whatman) using a glass funnel with a diameter of 3 mm under a gentle vacuum (<0.013 MPa), and the filters were subsequently rinsed with Milli-Q water to remove salts. We secured these filters with conductive carbon tape on a microscope stage before coating them with Pt-Pb alloy by vapor deposition using an MSP-1S magnetron spatter device (Vacuum Device). We set the Pt-Pb alloy-coated samples under an SEM (VE-8800, KEYENCE) and counted and identified diatoms in the samples following Hasle & Syvertsen (1997). The genus *Chaetoceros* was separately categorized into vegetative cells and resting spores. The biovolume (μm^3) of counted diatoms was estimated following Hillebrand et al. (1999).

2.4. DNA metabarcoding for diatom communities

A total of 290–1200 ml of seawater was filtered through a polycarbonate membrane (pore size 2.0 µm, diameter 25 mm; Merck) under a gentle vacuum (<0.013 MPa). The filters were immediately frozen at −80°C until DNA extraction. In the shore-based laboratory, we followed the bead-beating method described by Endo et al. (2013) to extract DNA from the filtered samples. We targeted the V4 region of the 18S rRNA gene to extract the amplicon via 2-step PCR. In the first PCR step, the targeted region was amplified by primers (Piredda et al. 2017) (forward: 5'-CCA GCA SCY GCG GTA ATT CC-3', reverse: 5'-ACT TTC GTT CTT GAT YRA TGA-3') with adaptor sequences (forward: 5'-ACA CTC TTT CCC TAC ACG ACG CTC TTC CGA TCT-3', reverse: 5'-GTG ACT GGA GTT CAG ACG TGT GCT CTT CCG ATC T-3'). The thermal cycling conditions for the first PCR step consisted of 3 intermediate steps after 2 min of incubation at 94°C: 30 cycles at 94°C for 30 s, 50°C for 30 s, and 72°C for 30 s. The cycle ended with a 72°C hold for 5 min. Here, we checked for contamination in the first PCR steps with negative controls of ultrapure water. The first PCR product was refined using AMPure XP beads (Beckman Coulter) before the second PCR step. The thermal cycling conditions for the second PCR involved 3 intermediate steps after the sample was held at 94°C for 2 min: 10 cycles at 94°C for 30 s, 60°C for 30 s, and 72°C for 30 s. The final stage of the second PCR step involved holding the sample at 72°C for 5 min. The amplicon libraries were purified using AMPure beads (Beckman Coulter), and the quality of the purified sample was checked via a Fragment Analyzer (Advanced Analytical Technologies) with the dsDNA 915 Reagent Kit. Finally, the amplicon libraries were sequenced with a MiSeq system (Illumina) using a MiSeq Reagent Kit v3 to create paired-end reads. The above library construction and sequencing were performed at the Bioengineering Lab Co., Ltd. (Sagamihara, Japan). The obtained nucleotide sequence data have been deposited with links to the BioProject accession number PRJDB17528 in the DDBJ BioProject database (https://www.ddbj.nig.ac.jp/bioproject/index-e.html).

The obtained sequence data were analyzed through QIIME2 (Bolyen et al. 2019) with the DADA2 plugin and the 'dada2 denoise-paired' command (Callahan et al. 2016). This analysis estimates amplicon sequence variants (ASVs). The ASVs were annotated by the Basic Local Alignment Search Tool (BLAST) using the Protist Ribosomal Reference (PR^2) database (Guillou et al. 2013) version 4.14.0 to convert taxonomy data.

2.5. Quantitative PCR (qPCR) for diatom-specific 18S rRNA gene

We quantified the copy numbers of the 18S rRNA gene in diatoms using a real-time PCR system (CFX Connect, Bio-Rad) employing the diatom-specific primer set described by Endo et al. (2018). Forward and reverse primers were 5'-AAC TAC TGC GAA

AGC ATT TA-3′ and 5′-GAC TAC GAT GGT ATC TRA TCA T-3′, respectively.

A standard curve for the 18S rRNA gene copy numbers was generated using linear plasmids containing artificial gene fragments (88 bp in length) of *Thalassiosira weissflogii* (Endo et al. 2018). The thermal cycling conditions for qPCR involved an initial 95°C hold for 1 min, followed by 40 cycles at 95°C for 5 s and 55°C for 60 s. In each qPCR analysis, we included a negative control of ultrapure water to check for any possible contamination.

2.6. Combining diatom data from DNA metabarcoding and SEM analyses

The absolute abundance (copy l^{-1}) of each ASV was calculated by multiplying the diatom-specific 18S rRNA gene abundance estimated via qPCR, and the abundance was adjusted by considering the relative contribution of the ASVs obtained from the DNA metabarcoding. Additionally, data from the SEM analysis and DNA metabarcoding were integrated to include information regarding resting spores of the genus *Chaetoceros* within the ASV-based diatom data set (see Section 4.1). Since Godhe et al. (2008) suggested that the biovolume of diatoms is significantly correlated with the copy number of the 18S rRNA gene in the organisms, we determined the copy number of the 18S rRNA gene from the genus *Chaetoceros* using the biovolume of vegetative cells and resting spores measured under SEM as follows:

$$\textit{Chaetoceros}\,\mathrm{VC}_{(\text{copy number})} = \textit{Chaetoceros}\,\mathrm{total}_{(\text{copy number})} \times \frac{\textit{Chaetoceros}\,\mathrm{VC}_{(\text{biovolume})}}{\textit{Chaetoceros}\,\mathrm{total}_{(\text{biovolume})}} \quad (1)$$

and

$$\textit{Chaetoceros}\,\mathrm{RS}_{(\text{copy number})} = \textit{Chaetoceros}\,\mathrm{total}_{(\text{copy number})} - \textit{Chaetoceros}\,\mathrm{VC}_{(\text{copy number})} \quad (2)$$

where VC and RS represent vegetative cells and resting spores, respectively. In the 3 SEM samples in which no *Chaetoceros* cells were detected, we defined the *Chaetoceros* $\mathrm{VC}_{(\text{biovolume})}$ / *Chaetoceros* $\mathrm{total}_{(\text{biovolume})}$ ratio as 1.

2.7. Diatom community diversity

Diversity in diatom communities was assessed by Pielou's evenness (J) index, a measure of species diversity from species evenness and species richness. The index ranges from 0, denoting the absence of evenness, to 1, representing full evenness. We calculated the index based on the absolute abundance (copies l^{-1}) of ASVs annotated at the species level. Note that the ASV data used for the calculation were not modified by the biovolume of the resting spores of *Chaetoceros* because we could not identify the resting spores of *Chaetoceros* at the species level via SEM.

2.8. Diatom community groups

Cluster analysis was applied to our modified ASV data set to reveal the horizontal distribution of the diatom community and infer the effects of environmental factors on the diatom community. High ranges of ASV abundance can have a greater influence on cluster analysis because the analysis employs a distance metric. Thus, we standardized the copy number data (X: copies l^{-1}) for each ASV by transformation to $\sqrt[4]{X}$ before the cluster analysis (Quinn & Keough 2002). Dissimilarities between samples were examined using the Bray-Curtis index based on the differences in the ASV composition. The dissimilarity indices are coupled to group the samples using hierarchical agglomerative clustering with a complete linkage method (an unweighted pair group method using the arithmetic mean).

To examine the intergroup differences in environmental factors and diatom community diversity, U-tests were conducted between the 2 main diatom community groups (Groups B and C, see Section 3.3), which were classified by cluster analysis. All statistical analyses were performed using R software version 4.3.0 (R Core Team 2023).

2.9. Daily current, turbidity, and chl *a* concentration near the bottom during autumn: mooring data

To further investigate the effect of wind on bottom current and microalgae in sediments, we analyzed the time series mooring data. Daily data of current, turbidity, and chl *a* near bottom in September and October from 2016 to 2019 were obtained from 2 temporally sequenced moorings in the Chukchi Shelf at Stn 35 with 58 m depth (Table S1). The moorings were deployed from 1 September 2016 to 19 September 2017 and from 19 September 2017 to 17 August 2020 (note that the first was a 1 yr mooring, whereas the other was a 3 yr mooring). An Aquadopp Current Meter

(NORTEK) and a turbidity and chl *a* sensor (ACLW-USB-Z, JFE Advantech) were located at 46 and 53 m depths, respectively. Wind speed from September to October from 2016 to 2019 was computed from the ERA5 hourly *u*- and *v*-wind components (Hersbach et al. 2023).

3. RESULTS

3.1. Environmental conditions of the study area during the cruise

Cool, fresh water overlaid warm, saline water in the upper layers of the shelf slope and basin (Stns 10–17 and 22–27 in Fig. 2). This cool, fresh water was classified as Ice Melt Water (IMW) and cool Coastal Water (cCW) (Danielson et al. 2020). The dominant source of fresh water in the low-salinity IMW and cCW was Sea-Ice Meltwater (SIM), which accounted for 6.1–13% (Fig. 3a). Consequently, the stratification index was high in the shelf slope and basin regions (Fig. 3b). On the other hand, warm Shelf Water (wSW) or cool Shelf Water (cSW) (Danielson et al. 2020) spread across the surface of the shelf region (Fig. 2), and the water column was weakly stratified (Fig. 3b).

Relatively strong winds were present across the study area during the cruise, especially in the shelf region (Fig. 4a; Fig. S1a) (see Section 3.3). In addition, the current speed was nearly uniform to the shallow sea bottom in the vertical direction (Fig. S1b).

The horizontal distributions of nutrients (NO_2 + NO_3, NH_4, $Si(OH)_4$, and PO_4) in the surface and subsurface layers were similar across the study area. The nutrient concentrations were relatively high on the southern shelf (NO_2 + NO_3 >3.3 µmol l^{-1}, NH_4 >3.5 µmol l^{-1}, $Si(OH)_4$ >18 µmol l^{-1}, PO_4 >1.2 µmol l^{-1}) and at 168° W, in contrast to the lower concentrations in the northern and eastern areas (NO_2 + NO_3 ~0.5 µmol l^{-1}, NH_4 ~0.6 µmol l^{-1}, $Si(OH)_4$ ~4.6 µmol l^{-1}, PO_4 ~0.5 µmol l^{-1}) (Fig. S2). In particular, not only nitrate and nitrite concentrations but also ammonium concentrations increased with the degradation of organic matter and were high (>3.5 µmol l^{-1}), even in the surface layers of the southern Chukchi shelf (Stns 31, 33, 34, and 35).

The shipboard measurements of PAR exhibited substantial daily variability, ranging from 0.51 to 5.89 mol photons m^{-2} d^{-1}, with an average of 2.32 ± 1.41 (SD) mol photons m^{-2} d^{-1} (Fig. S1c). Concurrently, the duration of daylight diminished throughout the cruise, with an average day length of 10.1 ± 0.94 h d^{-1}.

3.2. Chemotaxonomic community and diatom composition, abundance, and biovolume

Our study area had a relatively low chl *a* concentration (0.11–1.06 mg m^{-3}) with slight spatial variability (Fig. 5a,b). We decomposed the chl *a* concentration into 8 phytoplankton groups at the class level using the R package 'phytoclass' (Fig. 5c,d). The pigment/chl *a* ratio from our decomposition was comparable to that in a previous study (Zhuang et al. 2016) (Table S2). Diatoms were the dominant group across the study area, particularly from the southern shelf to the northern region of the Chukchi Sea, contributing up to 97.9% of the total chl *a* biomass (Fig. 5c,d). In contrast, the small-celled phytoplankton group prasinophytes sensu lato dominated at Stns 11 and 12 near the sea-ice-covered Canada Basin. A mixed community distribution was present on the southern shelf, where an elevated contribution of cryptophytes to the phytoplankton communities was observed. The variation in total chl *a* biomass was explained mainly by the diatom-derived chl *a* (Pearson, $p < 0.001$, $R^2 = 0.93$) (Fig. 6a).

We identified 14 genera of diatoms via SEM. The centric diatoms *Chaetoceros* spp. accounted for the highest percentage of biovolume in 21 samples, 6 of which were dominated by resting spores of *Chaetoceros* (Fig. S3a). The centric diatoms *Attheya* spp. and *Thalassiosira* spp. and the pennate diatom *Thalassionema nitzschioides* often dominated the other samples (Fig. S3a). *Proboscia* spp. were rare according to the SEM analysis.

We identified 21 genera of diatoms via DNA metabarcoding. The majority of the reads consisted of either *Proboscia* spp. or *Chaetoceros* spp. Several exceptions were found in the reads from Stns 11 and 12, where centric diatoms belonging to the Coscinodiscophyceae accounted for high percentages (Fig. S3b). Although 8 genera of pennate diatoms were identified, *Thalassionema* spp., which often appeared in SEM images, were not detected. Only 9 genera (i.e. *Attheya*, *Chaetoceros*, *Coscinodiscus*, *Ditylum*, *Proboscia*, *Rhizosolenia*, *Thalassiosira*, *Cylindrotheca*, *Fragilariopsis*) were identified by both SEM and DNA metabarcoding analyses.

The chl *a* biomass of diatoms correlated well with the copy number of the diatom-specific 18S rRNA gene (Pearson, $p < 0.001$, $R^2 = 0.66$) (Fig. 6b). In contrast, the diatom chl *a* concentration did not correlate well with the total biovolume of diatoms (Fig. 6c) or the copy number of diatom-specific 18S rRNA gene (Pearson, $p > 0.05$) (Fig. 6d), suggesting that the total biovolume may not adequately represent the diatom community.

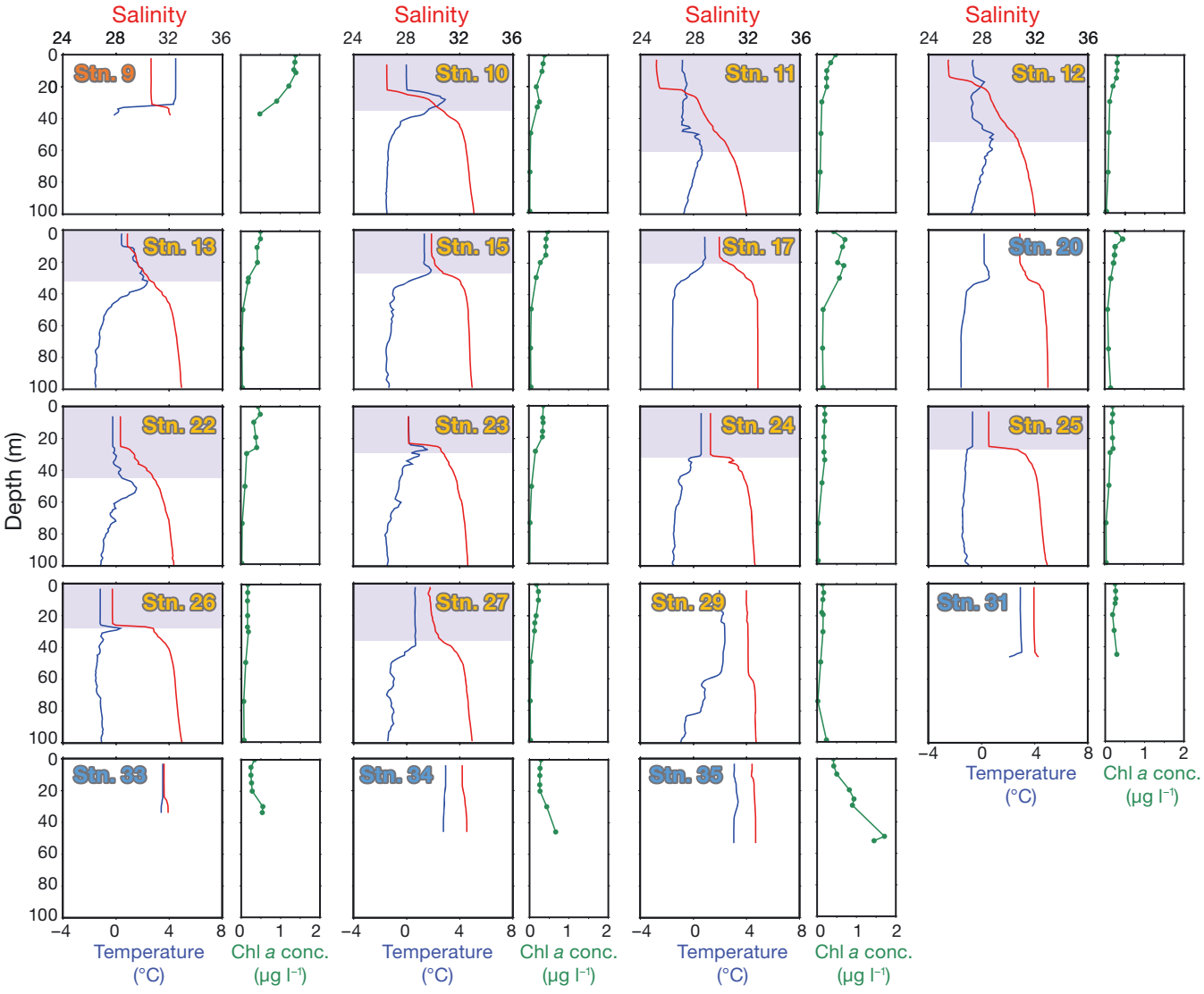

Fig. 2. Vertical profiles of temperature, salinity, and chlorophyll *a* (chl *a*) concentration. The color of the station number indicates the diatom community group classified by a cluster analysis (see Fig. 1). The purple boxes denote the layers with cold and low-salinity water, defined by Danielson et al. (2020) as Ice Melt Water and cool Coastal Water

3.3. Diatom community and relationships with environmental parameters

We classified the diatom community into 3 groups (A, B, C) based on the cluster analysis of the copy number of each ASV in the combined data (Fig. 1; Fig. S4). In addition to the outlier Group A (which included only Stn 9), Stn 20 seems to be a geographical outlier within Group C. The dominant diatom composition differed between Groups B and C; the contribution of *Proboscia* was the highest in Group B (Fig. 7a), while the resting spores of *Chaetoceros* (Fig. 7b,c) had the highest proportion in Group C (Fig. 7a). The ratio of the total number of resting spores to total cells of *Chaetoceros* was significantly greater in Group C (0.99 ± 0.03) than in Group B (0.55 ± 0.34) (*U*-test, $p < 0.001$; Figs. 4k & 7d). Group C was considered more diverse than Group B based on the *J* index (*U*-test, $p = 0.010$) (Fig. 7e). Group A represents the diatom distribution at Stn 9 (Fig. 1), where we observed the highest chl *a* concentration (Fig. 5c,d). Group B characterizes the diatom distribution in the shelf slope to basin regions, while Group C represents the diatom distribution on the shelf along 168.8° W and at Stn 20 (Fig. 1).

The environmental parameters also showed variations in the area corresponding to the classified diatom groups (Figs. 3b & 4a–i). Group B, which was found

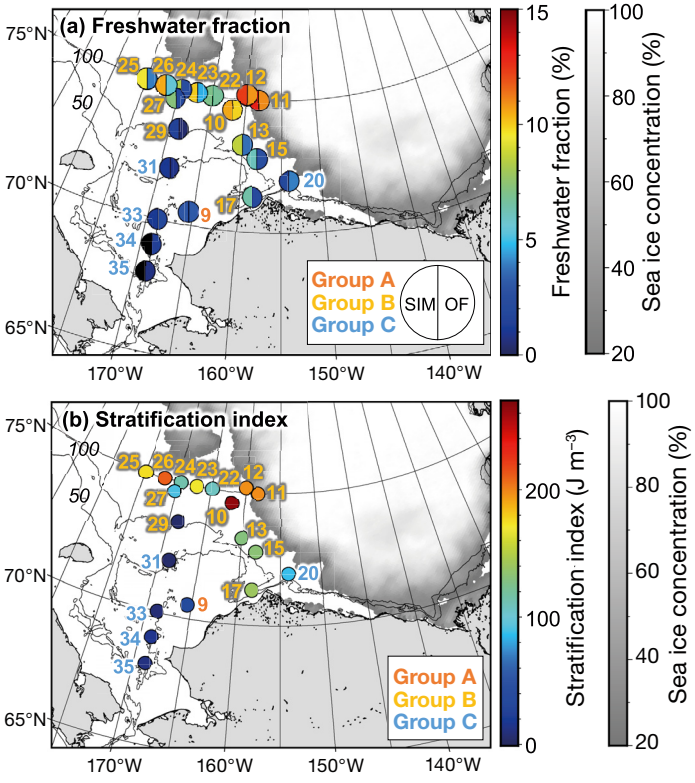

Fig. 3. (a) Freshwater fraction at 5 m depth at each station. The left and right part of the semicircles indicate the fractions of sea ice meltwater (SIM) and other fresh water (OF; consisting of precipitation, river runoff, and fresh water carried from the Pacific), respectively. The grayscale contours indicate the mean sea ice concentrations during the sampling period. The color of the station number indicates the diatom community group classified by a cluster analysis (see Fig. 1). (b) Stratification index (J m^{-3}) proposed as potential energy relative to the mixed state at each station (Ueno et al. 2020). The index was significantly higher in Group B than in Group C (*U*-test, p = 0.003)

closer to sea ice and was influenced by meltwater, seemed to prefer environments that were cooler, fresher, and had a higher stratification index (i.e. were more stable) (*U*-test, p = 0.003). On the other hand, Group C, representative of the shallower region, occupied environments with higher turbidity (i.e. lower beam transmission) and higher nutrient concentrations (NO_2 + NO_3, NH_4, $Si(OH)_4$, PO_4) (*U*-test, p < 0.001). In our study region, the observed current speed at the deepest layer, as measured by the ADCP, positively correlated with the ERA5-derived wind speed (Fig. 4j). Here, the observed current speed is defined as the median current speed for 1 h after the beginning of the observation at the deepest layer listed in Table S1. We filtered the wind speed and the bottom current speed to compute the correlation. The highest correlation of 0.25 (p = 0.002) was found with a 6 d moving average window (Fig. 4j; Fig. S5). The plots of Group C occupied the area of high wind and high current on the coordinate plane (Fig. 4j). In addition, the average wind speed was about 2 times higher in Group C than in Group B (*U*-test, p = 0.010, Fig. 4a). Note that the observed current speed of Group C (median = 22.4 cm s^{-1}) in the shallow region was much larger than the tidal current in the Chukchi Sea previously reported (1–5 cm s^{-1}) (Kawaguchi et al. 2015, Baumann et al. 2020). The diatom community groups exhibited a well-defined relationship with beam transmission and the chl *a* concentration (Fig. 4k). The low beam transmission (i.e. high turbidity) associated with Group C was not necessarily related to an increase in chl *a* concentration (Fig. 4k), suggesting that the high turbidity was caused mainly by particles other than phytoplankton with chl *a*.

3.4. Relationship between wind and bottom current, and the current, turbidity, and chl *a* in the Chukchi shelf from September to October

The 4 yr mooring and reanalysis data suggested that wind modulated the bottom current in the Chukchi shelf in autumn. The current speed near the bottom (24 h moving averaged value) correlated with the wind speed in September and October. The highest correlation coefficient was found when wind speed was averaged for 20 h with a 1 h lag between the current speed as a 4 yr average (p < 0.002 in all years, r = 0.56 for the 4 yr average; Figs. S6 & S7).

In turn, the instantaneous data of turbidity responded exponentially to that of current speed near the bottom (Fig. S8). However, the turbidity appeared to change by an order of magnitude during the 2018 observations (Fig. S9) which may have been caused by sensor drifting. Thus, we used data in 2016 and 2017, the first year of each mooring, for further analysis. As a result, the cumulative current speed over 13 h had the highest correlation with the turbidity near the bottom (24 h moving averaged value; p < 0.001, r = 0.38; Figs. S10 & S11). Furthermore, chl *a* concentration was accompanied by turbidity (p = 0.001, r = 0.37; Fig. S11). Thus, the bottom current modulated by wind could drive the resuspension of microalgae in sediments from the seafloor.

4. DISCUSSION

4.1. Comparison of diatom composition between SEM and DNA techniques

Biovolume is significantly correlated with the copy number of the 18S rRNA gene in diatoms (Godhe et

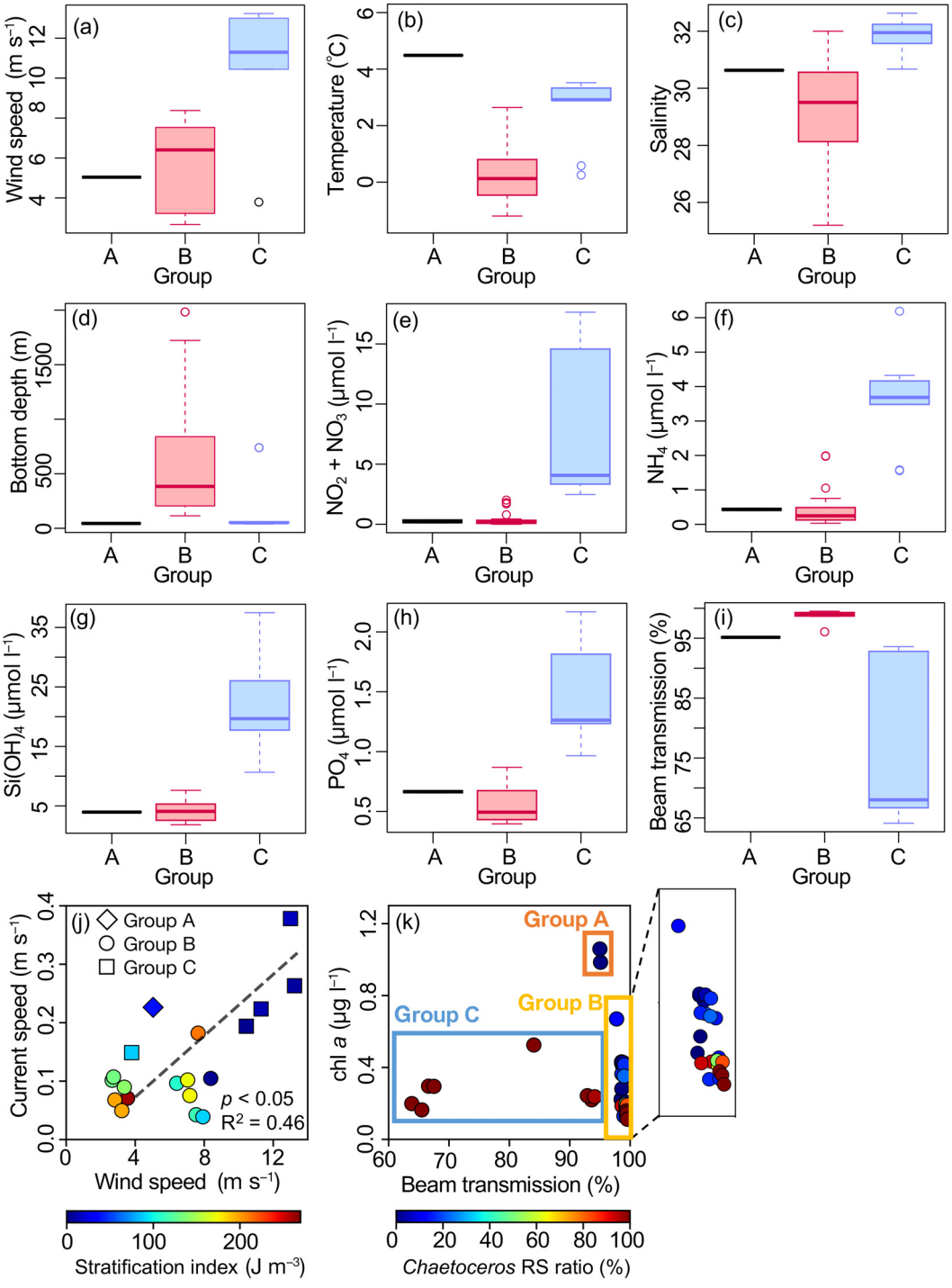

Fig. 4. (a–i) Environmental factors of each diatom community group. The boxes represent the interquartile range (25th to 75th percentile) of the data, the line within each box is the median, the whiskers show the range of the data from the minimum to the maximum values and the open circles are outliers. (a) Six day average wind speeds before observations of each diatom community group, (b) temperature, (c) salinity, (d) bottom depth, (e) $NO_2 + NO_3$ concentration, (f) NH_4 concentration, (g) $Si(OH)_4$ concentration, (h) PO_4 concentration, and (i) beam transmission. The different colors of the boxplots indicate significant differences between Groups B and C (i.e. *U*-test, $p < 0.01$). (j) Relationships between wind speed (6 d average wind speeds before observations) and current speed at the deepest layer (median current speed at the deepest layer for 1 h after the beginning of the observation). The color bar indicates the stratification index, and the shapes of the plots represent the diatom community group classified by cluster analysis (see Fig. 1). (k) Relationships between beam transmission and chlorophyll *a* (chl *a*) concentration. The color bar indicates the ratio of the abundance of resting spores (RS) of *Chaetoceros* to total cells

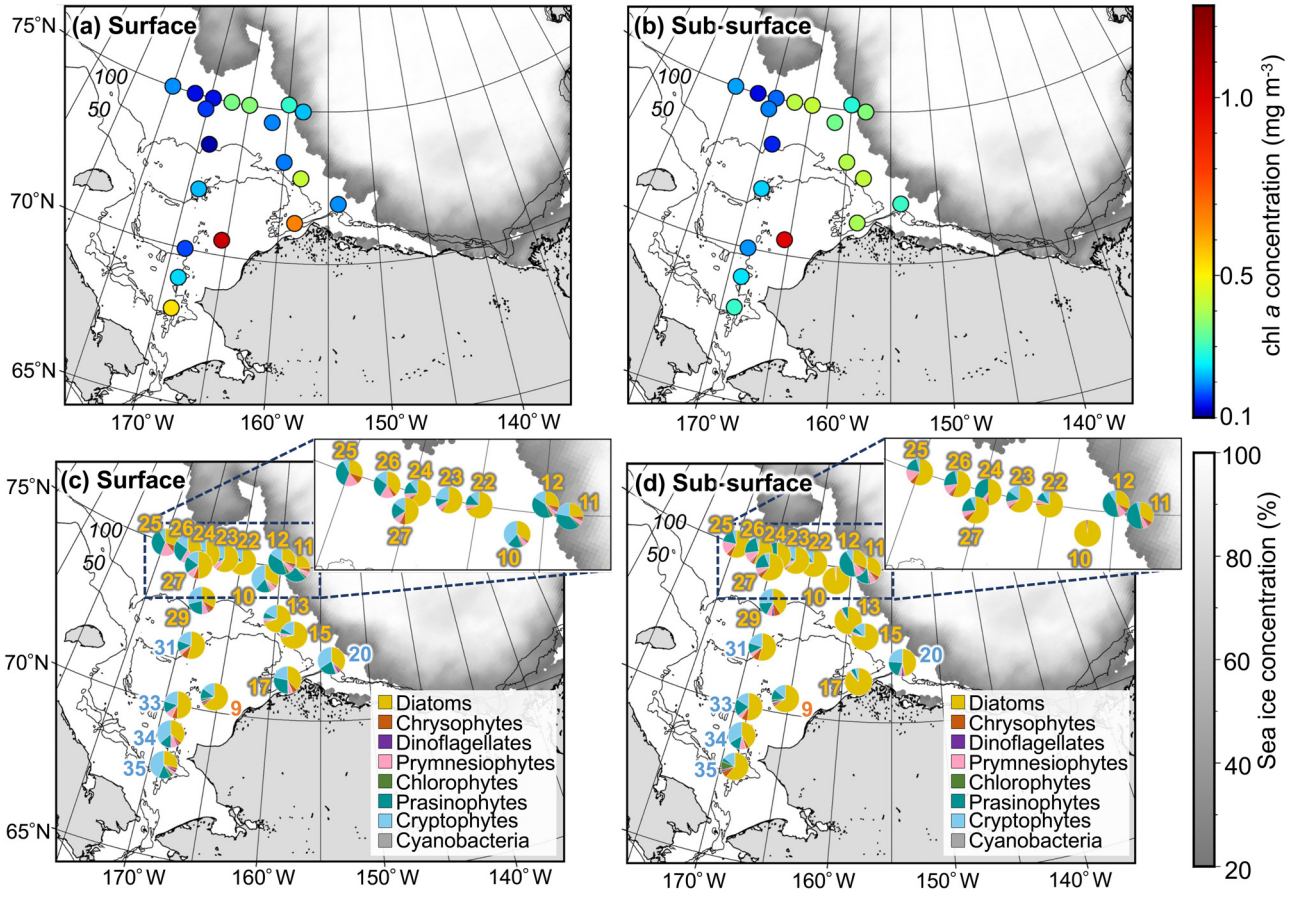

Fig. 5. Spatial distribution of the total chlorophyll *a* (chl *a*) concentration and contribution of each phytoplankton taxonomic group to the chl *a* biomass at the (a,c) surface and (b,d) subsurface. The phytoplankton taxonomic contribution was revealed by a pigment-based chemotaxonomic tool using the R software package 'phytoclass'. The grayscale contours indicate the mean sea ice concentrations during the sampling period. The color of the station number indicates the diatom community group classified by cluster analysis (see Fig. 1). While there were some horizontal variations in phytoplankton community composition over all groups, diatoms were the primary factor explaining the changes in the total phytoplankton biomass

al. 2008). However, our study demonstrated that diatom biovolume was not strongly related to the copy number of the diatom-specific 18S rRNA gene. The results could be due to either an overestimation of the 18S rRNA gene copy number or an underestimation of the diatom biovolume. Our diatom biovolume was likely underestimated due to the strong correlation between the copy number of the diatom-specific 18S rRNA gene and the diatom-derived chl *a* concentration. Therefore, at least in the present study, we concluded that DNA metabarcoding data are more reliable than SEM data for assessing diatom communities. The volume of seawater used for analysis differed between the SEM (107–120 ml) and metabarcoding (1200 ml) techniques, which could lead to disagreement with the diatom community between the analytical methods (Fig. S3).

Proboscia often dominates diatom assemblages on the Pacific Arctic shelf during autumn (Matsuno et al. 2014). We employed 2 methods to estimate the abundance of *Proboscia*: DNA metabarcoding and SEM data. These 2 methods yielded completely different results. Although *Proboscia* were rarely detected in any SEM samples, they were often predominant in DNA metabarcoding samples. Since *Proboscia* species are large, long diatoms with cell lengths of more than 220 µm (Hasle & Syvertsen 1997, Kulk et al. 2019) and because their silicate frustules are thin (Sukhanova et al. 2006), the filtration process to prepare samples for SEM analysis could damage the long cells of *Proboscia*. Many unidentified or uncounted fragments in the samples might have been broken *Proboscia* cells. As a result, we may have overestimated the contribution of other centric diatoms, especially *Chaetoceros* spp., to the diatom abundance and biomass.

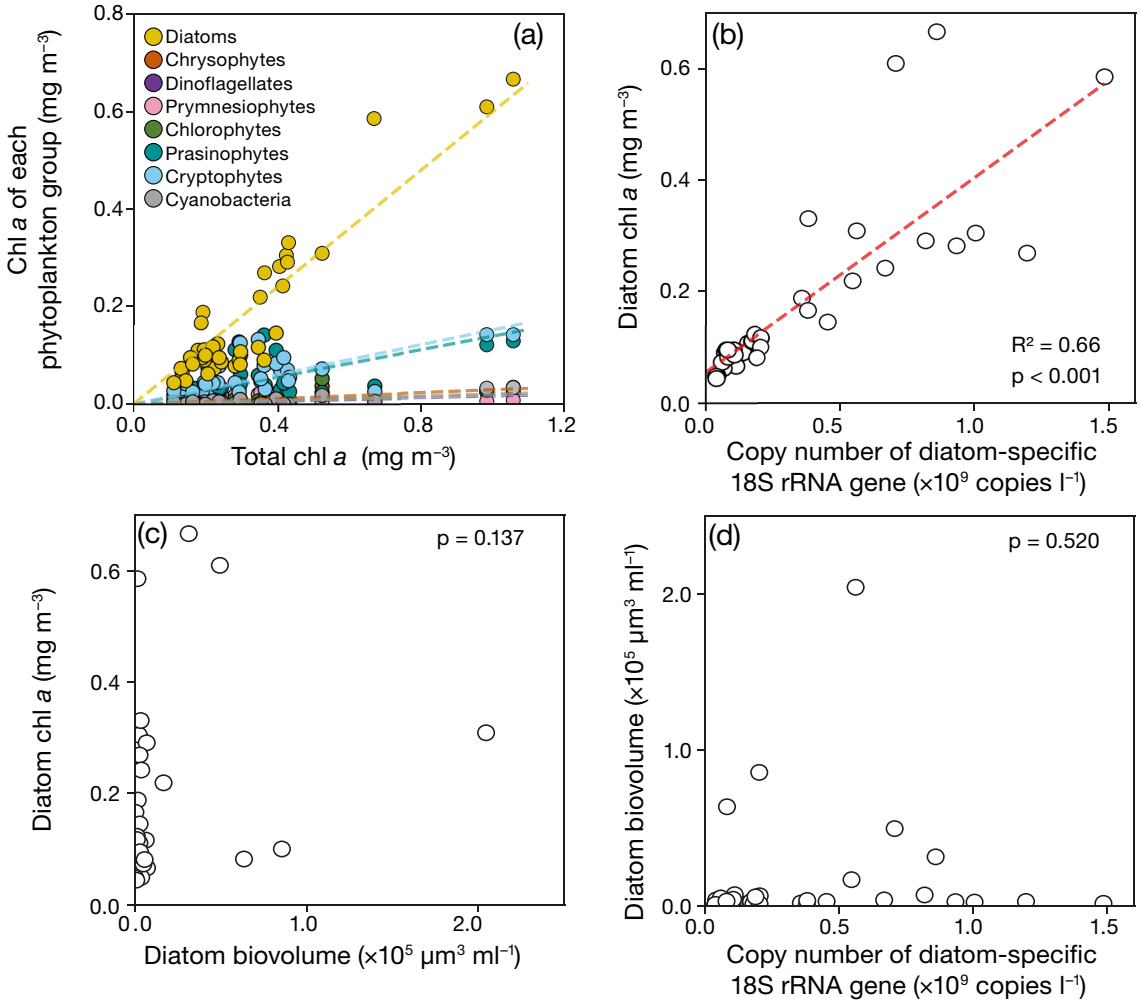

Fig. 6. Relationships between: (a) total chlorophyll *a* (chl *a*) concentration and diatom-derived chl *a* concentration estimated by the pigment-based chemotaxonomic tool 'phytoclass'; (b) copy number of diatom-specific 18S rRNA gene and diatom-derived chl *a* concentration; (c) diatom biovolume estimated using scanning electron microscopy (SEM) and diatom chl *a* concentration; and (d) copy number of diatom-specific 18S rRNA gene and diatom biovolume

SEM analysis can detect diatom resting spores based on morphological differences, whereas it is not possible to differentiate vegetative cells from resting spores based on the 18S rRNA gene sequence. Diatoms form thick frustules when becoming resting spores, and the sinking of resting spores occurs faster than the sinking of vegetative cells (McQuoid & Hobson 1996). These sinking diatom resting spores play an essential role in the POC flux (Rynearson et al. 2013). Thus, it is crucial to assess vegetative cells and resting spores separately. We modified the ASV data by incorporating the *Chaetoceros* resting spore data (see Section 2.6). Based on the modified data set, the diatom communities in the Chukchi Sea during autumn were characterized by *Proboscia* and the resting spores of *Chaetoceros*. In addition, the advantages of DNA metabarcoding and SEM analyses were well demonstrated in the quantification of *Proboscia* by DNA metabarcoding and the detection of resting spores by SEM. In the present study, we suggest the usefulness of ASV data sets that incorporate resting spore data, especially for shallow shelf regions with abundant resting spores.

4.2. Phytoplankton community structure during autumn

The spatial distribution of the phytoplankton community structure in our data coincided with typical patterns in the post-bloom season in the Pacific Arctic (Coupel et al. 2012, 2015, Joo et al. 2022). During late autumn, a distinctive characteristic observed in the shelf region was the prevalence of diatoms despite

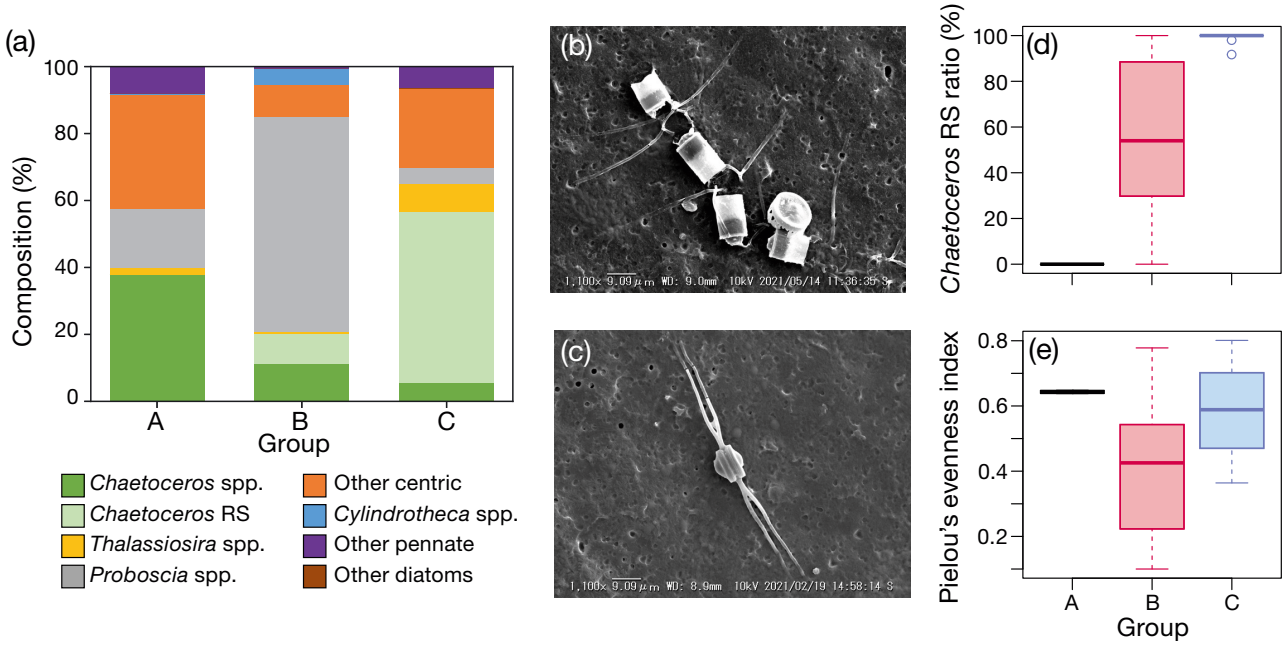

Fig. 7. (a) Diatom composition of each community group classified by cluster analysis (see Fig. 1). (b,c) Photographs of *Chaetoceros* spp. resting spores observed via SEM at 1100× magnification. (d) Abundance ratio of the resting spores (RS) of *Chaetoceros* to total cells in each group and (e) diatom community diversity (Pielou's evenness index) of each group. The different colors of the boxplots indicate significant differences between Groups B and C (*U*-test, $p < 0.01$). Box plot parameters as in Fig. 4

low chl *a* concentration coupled with a localized contribution of cryptophytes to the phytoplankton communities. Within the cryptophytes, previous studies reported that *Cryptomonas* sp. sometimes contributes to the phytoplankton community in the Chukchi Sea (Sukhanova et al. 2009). In contrast, at stations near sea ice in the Canada Basin, prasinophytes sensu lato dominated the waters affected by meltwater, consistent with previous observations that identified *Micromonus* sp. (Coupel et al. 2012). While there were some horizontal variations in phytoplankton community composition, diatoms were the primary factor explaining the changes in the total phytoplankton biomass.

The variability within a diatom assemblage can be characterized by environmental properties. The southern Chukchi Sea was characterized by shallow, highly turbid, and weakly stratified water columns, and a diverse diatom community with abundant resting spores of *Chaetoceros* was present. Subsurface mixing by strong wind events in this region is known to homogenize the water column and increase the phytoplankton biomass (Kawaguchi et al. 2015, Nishino et al. 2015). Previous studies have reported that numerous viable *Chaetoceros* cells are present on the seafloor of the Chukchi shelf (Tsukazaki et al. 2018, Fukai et al. 2021, 2022, Peng et al. 2023), and most of these cells are resting spores (Fukai et al. 2022). The wind and the current at the deepest layer were higher in the region where the resting spores were abundant in the surface (Fig. 4j). Furthermore, the time series observation at the fixed station in the Chukchi shelf clearly suggested potential linkages between the wind and the current, turbidity, and chl *a* concentration near the bottom during autumn. The wind can modulate the bottom current, which would lead to a release of the sediment with microalgae into the ocean interior. These results are consistent with a previous study in the Bering Strait showing that surface winds modulate barotropic currents, and the strong currents, in turn, trigger high-turbidity events with high chl *a* releases (Abe et al. 2019). Thus, although we did not observe it directly during the cruise in 2020, the evidence from the mooring and reanalysis data led us to speculate that strong winds enhanced the currents within the benthic boundary layer, which entrains *Chaetoceros* resting spore-rich sediments and nutrients (including NH_4) to the ocean interior. Since the Chukchi shelf was weakly stratified (Fig. 4j) and the current speed was nearly uniform to the shallow sea bottom in the vertical direction (Fig. S1b), there might be vertical mixing to transport resuspended *Chaetoceros* resting spores to the surface. The cruise across the Chukchi shelf revealed that such resuspension of diatoms from the bottom would occur over a wide area of the region. On the other

hand, the time series data suggested that the response of seafloor sediments and microalgae to wind-modulated currents would commonly happen during autumn. Therefore, our multiple observations show that diatoms in the sediments could generally be transported to the sunlit surface of the Chukchi shelf during autumn.

The other diatom Group B was distributed in a completely different environment characterized by cool, fresh water, including sea-ice meltwater at the surface. The surface layer and SSL in this region exhibited stronger stratification than the region dominated by Group C, and *Proboscia*, a typical diatom of the Pacific Arctic during autumn (Matsuno et al. 2014), was predominant. The strong stratification in this area could not be destroyed by the moderate winds (6.4 m s^{-1} as the station-median 6 d mean speed before observation) blowing prior to our sampling according to a previous study (Nishino et al. 2020). Nishino et al. (2020) suggested that the seasonal pycnocline formed by melting sea ice in autumn is strong enough to impede vertical mixing within the upper 20 m, even in the presence of wind speeds above 12 m s^{-1}. Furthermore, because the nutricline is located deeper than the euphotic layer, there is no effective mechanism for supplying nutrients from below the pycnocline to the diatom community in the autumn water column. As a result, typical microalgae, such as *Proboscia,* were ubiquitous near the surface.

4.3. Possible impact of strong winds on the phenology of the diatom community during autumn on the Chukchi shelf

The frequency and intensity of autumn storms have been increasing in this area due to the decreasing extent of sea ice in this region (Long & Perrie 2012, Ardyna et al. 2014). It has also been reported that autumn phytoplankton blooms are becoming more common (Ardyna et al. 2014). Changes in environmental factors can alter the phenology of primary production. We observed resting spores of *Chaetoceros* at the surface and speculate that they were resuspended from the seafloor (Fig. 8a). A previous study based on fixed-point observations in a similar region indicated that intense gale-force winds (>10 m s^{-1}) increased upward nutrient fluxes, which supported primary production and resulted in increased phytoplankton biomass (Nishino et al. 2015). Consistent with this past study, our observation revealed a high nutrient content, including NH_4, at the surface in the shelf region and thus available for microalgae for photosynthesis. Our findings suggest that viable diatoms sourced from the seafloor can increase the initial biomass and trigger an autumn bloom. Such diatom input from the seafloor has the potential to transform into a scenario of diatom community succession during autumn (Fig. 8a,b). Diatom resuspension from the seafloor can increase the initial diatom population available for a bloom, accelerating the time to reach an autumn bloom state (Fig. 8c). The decrease in the time required to form a bloom can be advantageous for Arctic ecosystems in autumn when primary production ceases due to the extent of sea ice coverage and decreasing solar radiation. Furthermore, the seeding potential of diatoms in sediments needs to be considered. Viable diatoms in sediments on the Chukchi shelf are known to resume productivity within a few days of receiving sufficient light (30 µmol photons m^{-2} s^{-1} with a 12:12 h light:dark cycle) based on sediment samples from the same cruise (Fukai et al. 2022). The light setting in these laboratory experiments was comparable to the mean surface daily PAR during the cruise (2.32 mol photons m^{-2} d^{-1}), which was equivalent to the value of 1.30 mol photons m^{-2} d^{-1}. Shiozaki et al. (2022) also showed an increase in diatom communities on the Chukchi shelf under limited light availability (0.384 mol photons m^{-2} d^{-1}). These past studies and our current study suggest that diatoms from the seafloor have significant seeding potential for autumn primary production. Diatoms originating from the seafloor may be responsible for phenological changes in phytoplankton communities on the Chukchi shelf during autumn.

5. CONCLUSIONS

We characterized the diatom community during the autumn in the Chukchi Sea using a modified diatom data set constructed through DNA metabarcoding and SEM analyses. The SEM analysis underestimated *Proboscia*, and DNA metabarcoding had difficulty in differentiating vegetative diatom cells from resting spores. Our objective was to characterize the diatom assemblages of the resting spores of *Chaetoceros* and *Proboscia* throughout the study area, and combining DNA metabarcoding and SEM data was advantageous for our analysis.

We revealed 2 types of oceanographical and microalgal features in the Chukchi Sea during autumn. The predominant diatoms in the northern and eastern regions were typical autumn diatoms. The water depths in these regions were deep, and the presence of meltwater resulted in strong stratification. A strong wind

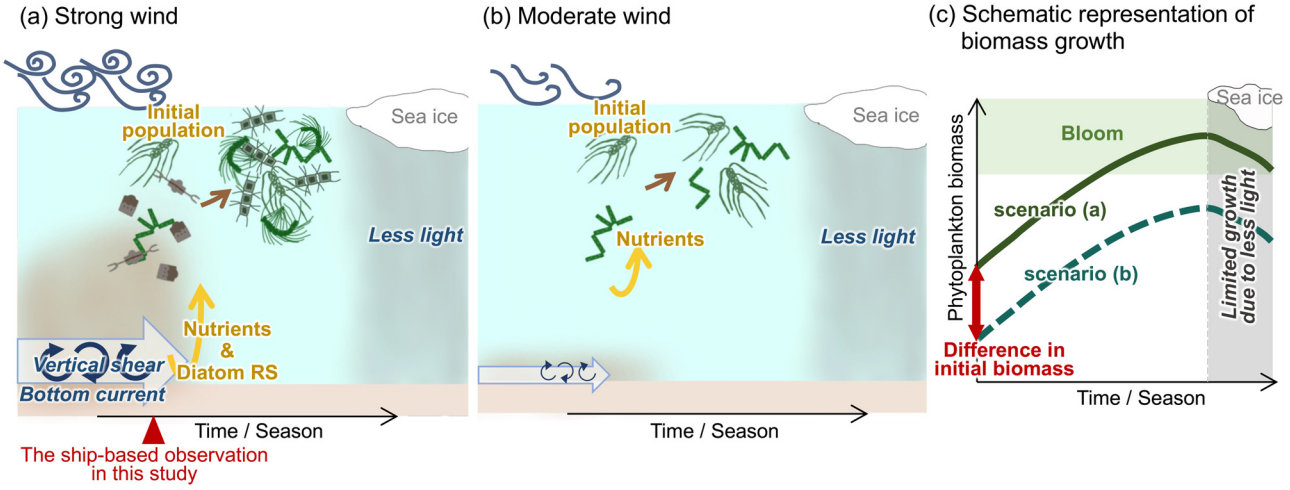

Fig. 8. Potential diatom community succession during autumn on the Chukchi shelf. (a) As our observational evidence indicates, the bottom current in the shallow sea responds to strong winds, resulting in the resuspension of diatoms in sediments. The enhanced mixing in the weakly stratified water column could supply nutrients and the resuspended diatoms to the upper water. RS: resting spores. (b) The response at the bottom is reduced when the wind subsides. There is no extra supply of initial biomass from diatoms on the seafloor. (c) Evolution of phytoplankton biomass under the scenarios in illustrated in panels (a) and (b)

event did not strengthen the diatom community structure in surface or deep waters. In contrast, the wind modulated the bottom current, which led to the resuspension of sediments and microalgae into the ocean interior. Thus, we speculated that the diatom community in the southern Chukchi shelf can be transported from the seafloor during periods of strong winds. This linkage between the upper and bottom community structures was probably supported by the dominant presence of Group C and many resting spores of *Chaetoceros*. Because diatoms in sediments can proliferate after light exposure (Fukai et al. 2022, Pinder & Töpel 2022, Shiozaki et al. 2022), we envisage that they can contribute to primary production in the sunlit surface layer. Additionally, based on the multiple data from the cruise and the moorings, we propose that such resuspension of sediments and microalgae from the seafloor could commonly occur over the Chukchi shelf during autumn.

The impact of wind-induced stress on the ocean has intensified owing to the recent delay in sea ice formation and the higher frequency of storms (Ardyna et al. 2014), leading to the redistribution of settled diatoms into the water column on shallow Arctic shelves. The resuspension of settled diatoms can contribute to phenological shifts in phytoplankton communities within the Chukchi shelf in autumn. From an ecological perspective, pulsed diatom biomass provides a favorable feeding environment for phytoplankton grazers (Matsuno et al. 2015, Fujiwara et al. 2018). The developmental success of phytoplankton grazers depends on food quality and the duration of the food supply before diapausing for winter (Feng et al. 2018). While the food supply from autumn primary production is increasing, the detailed energy pathways leading to higher trophic levels are poorly constrained. There is a need to better quantify autumn ecosystem activity across the food chain in the changing Arctic.

Acknowledgements. We thank the captain, crew, and researchers aboard the RV 'Mirai' (JAMSTEC) for their tremendous efforts during the field sampling. We also thank the staff of Marine Works Japan, Ltd., for their skillful work aboard the ship and for data processing. We extend our gratitude to Kohei Matsuno and Koki Tokuhiro for their support during the 'Mirai' cruise. The present work was part of Y.F.'s PhD thesis. This work was supported by the Japan Society for the Promotion of Science (JSPS) KAKENHI (grant numbers JP20J20410, JP21H03583, JP23K20031, JP23H03516), the Japan Science and Technology Agency (JST) CREST (JPMJCR23J4), and the Arctic Challenge for Sustainability II (ArCSII) project (program grant number JPMXD1420318865).

LITERATURE CITED

Abe H, Sampei M, Hirawake T, Waga H, Nishino S, Ooki A (2019) Sediment-associated phytoplankton release from the seafloor in response to wind-induced barotropic currents in the Bering Strait. Front Mar Sci 6:97

Ardyna M, Babin M, Gosselin M, Devred E, Rainville L, Tremblay JÉ (2014) Recent Arctic Ocean sea ice loss triggers novel fall phytoplankton blooms. Geophys Res Lett 41:6207–6212

Balzano S, Percopo I, Siano R, Gourvil P and others (2017) Morphological and genetic diversity of Beaufort Sea diatoms with high contributions from the *Chaetoceros neogracilis* species complex. J Phycol 53:161–187

Baumann TM, Polyakov IV, Padman L, Danielson S and others (2020) Arctic tidal current atlas. Sci Data 7:275

Bolyen E, Rideout JR, Dillon MR, Bokulich NA and others (2019) Reproducible, interactive, scalable and extensible microbiome data science using QIIME 2. Nat Biotechnol 37:852–857

Callahan BJ, McMurdie PJ, Rosen MJ, Han AW, Johnson AJA, Holmes SP (2016) DADA2: high-resolution sample inference from Illumina amplicon data. Nat Methods 13: 581–583

Coupel P, Jin HY, Joo M, Horner R and others (2012) Phytoplankton distribution in unusually low sea ice cover over the Pacific Arctic. Biogeosciences 9:4835–4850

Coupel P, Matsuoka A, Ruiz-Pino D, Gosselin M, Marie D, Tremblay JÉ, Babin M (2015) Pigment signatures of phytoplankton communities in the Beaufort Sea. Biogeosciences 12:991–1006

Danielson SL, Ahkinga O, Ashjian C, Basyuk E and others (2020) Manifestation and consequences of warming and altered heat fluxes over the Bering and Chukchi Sea continental shelves. Deep Sea Res II 177:104781

Endo H, Yoshimura T, Kataoka T, Suzuki K (2013) Effects of CO_2 and iron availability on phytoplankton and eubacterial community compositions in the northwest subarctic Pacific. J Exp Mar Biol Ecol 439:160–175

Endo H, Ogata H, Suzuki K (2018) Contrasting biogeography and diversity patterns between diatoms and haptophytes in the central Pacific Ocean. Sci Rep 8:10916

Fang YC, Janout M, Kawaguchi Y, Statscewich H (2022) Semidiurnal internal tides observed on the eastern flank of Hanna Shoal in the northeastern Chukchi Sea. J Geophys Res Oceans 127:e2021JC018232

Feng Z, Ji R, Ashjian C, Campbell R, Zhang J (2018) Biogeographic responses of the copepod *Calanus glacialis* to a changing Arctic marine environment. Glob Change Biol 24:e159–e170

Fujiwara A, Hirawake T, Suzuki K, Imai I, Saitoh SI (2014) Timing of sea ice retreat can alter phytoplankton community structure in the western Arctic Ocean. Biogeosciences 11: 1705–1716

Fujiwara A, Nishino S, Matsuno K, Onodera J and others (2018) Changes in phytoplankton community structure during wind-induced fall bloom on the central Chukchi shelf. Polar Biol 41:1279–1295

Fukai Y, Matsuno K, Fujiwara A, Suzuki K, Richlen ML, Fachon E, Anderson DM (2021) Impact of sea-ice dynamics on the spatial distribution of diatom resting stages in sediments of the Pacific Arctic Region. J Geophys Res Oceans 126:e2021JC017223

Fukai Y, Matsuno K, Fujiwara A, Suzuki K (2022) Photophysiological response of diatoms in surface sediments to light exposure: a laboratory experiment on a diatom community in sediments from the Chukchi Sea. Front Mar Sci 9:998711

Gérikas Ribeiro C, dos Santos AL, Gourvil P, Le Gall F and others (2020) Culturable diversity of Arctic phytoplankton during pack ice melting. Elementa Sci Anthropocene 8:6

Giesbrecht KE, Varela DE, Wiktor J, Grebmeier JM, Kelly B, Long JE (2019) A decade of summertime measurements of phytoplankton biomass, productivity and assemblage composition in the Pacific Arctic Region from 2006 to 2016. Deep Sea Res II 162:93–113

Godhe A, Asplund ME, Härnström K, Saravanan V, Tyagi A, Karunasagar I (2008) Quantification of diatom and dinoflagellate biomasses in coastal marine seawater samples by real-time PCR. Appl Environ Microbiol 74: 7174–7182

Guillou L, Bachar D, Audic S, Bass D and others (2013) The Protist Ribosomal Reference database (PR2): a catalog of unicellular eukaryote small sub-unit rRNA sequences with curated taxonomy. Nucleic Acids Res 41:D597–D604

Hargraves PE, French FW (1983) Diatom resting spores: significance and strategies. In: Fryxell GA (ed) Survival strategies of the algae. Cambridge University Press, New York, NY, p 49–68

Hasle GR, Syvertsen EE (1997) Marine diatoms. In: Tomas CR (ed) Identifying marine phytoplankton. Academic Press, San Diego, CA, p 5–385

Hayward A, Pinkerton MH, Gutierrez-Rodriguez A (2023) Phytoclass: a pigment-based chemotaxonomic method to determine the biomass of phytoplankton classes. Limnol Oceanogr Methods 21:220–241

Hersbach H, Bell B, Berrisford P, Biavati G and others (2023) ERA5 hourly data on pressure levels from 1940 to present. Copernicus Climate Change Service (C3S) Climate Data Store (CDS). https://doi.org/10.24381/cds.bd0915c6 (accessed 1 February 2024)

Hill V, Ardyna M, Lee SH, Varela DE (2018) Decadal trends in phytoplankton production in the Pacific Arctic Region from 1950 to 2012. Deep Sea Res II 152:82–94

Hillebrand H, Dürselen CD, Kirschtel D, Pollingher U, Zohary T (1999) Biovolume calculation for pelagic and benthic microalgae. J Phycol 35:403–424

Hoppenrath M, Elbrächter M, Drebes G (2009) Marine phytoplankton: selected microphytoplankton species from the North Sea around Helgoland and Sylt. Schweizerbart Science Publishers, Frankfurt

Joo HM, Kim KE, Park JS, Kim HJ and others (2022) Ecological responses of core phytoplankton by latitudinal differences in the Arctic Ocean in late summer revealed by 18S rDNA metabarcoding. Front Mar Sci 9:879911

Kawaguchi Y, Nishino S, Inoue J (2015) Fixed-point observation of mixed layer evolution in the seasonally ice-free Chukchi Sea: turbulent mixing due to gale winds and internal gravity waves. J Phys Oceanogr 45:836–853

Kulk G, Buist A, van de Poll WH, Rozema PD, Buma AGJ (2019) Size scaling of photophysiology and growth in four freshly isolated diatom species from Ryder Bay, western Antarctic peninsula. J Phycol 55:314–328

Kuwata A, Hama T, Takahashi M (1993) Ecophysiological characterization of two life forms, resting spores and resting cells, of a marine planktonic diatom, *Chaetoceros pseudocurvisetus*, formed under nutrient depletion. Mar Ecol Prog Ser 102:245–255

Lalande C, Grebmeier JM, Hopcroft RR, Danielson SL (2020) Annual cycle of export fluxes of biogenic matter near Hanna Shoal in the northeast Chukchi Sea. Deep Sea Res II 177:104730

Long Z, Perrie W (2012) Air-sea interactions during an Arctic storm. J Geophys Res Atmos 117:D15103

Lopes dos Santos A, Gérikas Ribeiro C, Ong D, Garczarek L and others (2022) Phytoplankton diversity and ecology through the lens of high throughput sequencing technologies. In: Clementson LA, Eriksen RS, Willis A (eds) Advances in phytoplankton ecology. Elsevier, Amsterdam, p 353–413

Matsuno K, Ichinomiya M, Yamaguchi A, Imai I, Kikuchi T (2014) Horizontal distribution of microprotist community structure in the western Arctic Ocean during late summer and early fall of 2010. Polar Biol 37:1185–1195

Matsuno K, Yamaguchi A, Nishino S, Inoue J, Kikuchi T (2015) Short-term changes in the mesozooplankton community and copepod gut pigment in the Chukchi Sea in autumn: reflections of a strong wind event. Biogeosciences 12:4005–4015

McQuoid MR, Hobson LA (1996) Diatom resting stages. J Phycol 32:889–902
Nishino S (2020) R/V *Mirai* cruise report, MR20-05C. JAMSTEC, Yokosuka. https://www.godac.jamstec.go.jp/darwin/en/index.html
Nishino S, Kawaguchi Y, Inoue J, Hirawake T and others (2015) Nutrient supply and biological response to wind-induced mixing, inertial motion, internal waves, and currents in the northern Chukchi Sea. J Geophys Res Oceans 120:1975–1992
Nishino S, Kikuchi T, Fujiwara A, Hirawake T, Aoyama M (2016) Water mass characteristics and their temporal changes in a biological hotspot in the southern Chukchi Sea. Biogeosciences 13:2563–2578
Nishino S, Kawaguchi Y, Inoue J, Yamamoto-Kawai M, Aoyama M, Harada N, Kikuchi T (2020) Do strong winds impact water mass, nutrient, and phytoplankton distributions in the ice-free Canada Basin in the fall? J Geophys Res Oceans 125:e2019JC015428
Peng L, Xie C, Wang M, Gu J and others (2023) Metabarcoding of microeukaryotes in surface sediments from the Pacific Arctic and adjacent sea areas: the role of diatoms in the biological pump. Global Planet Change 230:104262
Pinder MIM, Töpel M (2022) Ancient diatom DNA. In: Falciatore A, Mock T (eds) The molecular life of diatoms. Springer International Publishing, Cham, p 87–108
Piredda R, Tomasino MP, D'Erchia AM, Manzari C and others (2017) Diversity and temporal patterns of planktonic protist assemblages at a Mediterranean Long Term Ecological Research site. FEMS Microbiol Ecol 93:fiw200
Quinn GP, Keough MJ (2002) Experimental design and data analysis for biologists. Cambridge University Press, New York, NY
R Core Team (2023) R: a language and environment for statistical computing. R Foundation for Statistical Computing, Vienna
Rynearson TA, Richardson K, Lampitt RS, Sieracki ME, Poulton AJ, Lyngsgaard MM, Perry MJ (2013) Major contribution of diatom resting spores to vertical flux in the subpolar North Atlantic. Deep Sea Res I 82:60–71
Sergeeva VM, Sukhanova IN, Flint MV, Pautova LA, Grebmeier JM, Cooper LW (2010) Phytoplankton community in the Western Arctic in July–August 2003. Oceanology 50:184–197
Shiozaki T, Fujiwara A, Sugie K, Nishino S, Makabe A, Harada N (2022) Bottom-associated phytoplankton bloom and its expansion in the Arctic Ocean. Glob Change Biol 28:7286–7295
Springer AM, McRoy CP, Flint MV (1996) The Bering Sea Green Belt: shelf-edge processes and ecosystem production. Fish Oceanogr 5:205–223
Sukhanova IN, Flint MV, Whitledge TE, Stockwell DA, Rho TK (2006) Mass development of the planktonic diatom *Proboscia alata* over the Bering Sea shelf in the summer season. Oceanology 46:200–216
Sukhanova IN, Flint MV, Pautova LA, Stockwell DA, Grebmeier JM, Sergeeva VM (2009) Phytoplankton of the western Arctic in the spring and summer of 2002: structure and seasonal changes. Deep Sea Res II 56:1223–1236
Sundqvist L, Godhe A, Jonsson PR, Sefbom J (2018) The anchoring effect—long-term dormancy and genetic population structure. ISME J 12:2929–2941
Šupraha L, Klemm K, Gran-Stadniczeñko S, Hörstmann C, Vaulot D, Edvardsen B, John U (2022) Diversity and biogeography of planktonic diatoms in Svalbard fjords: the role of dispersal and Arctic endemism in phytoplankton community structuring. Elementa Sci Anthropocene 10:00117
Suzuki K, Kamimura A, Hooker SB (2015) Rapid and highly sensitive analysis of chlorophylls and carotenoids from marine phytoplankton using ultra-high performance liquid chromatography (UHPLC) with the first derivative spectrum chromatogram (FDSC) technique. Mar Chem 176:96–109
Suzuki K, Yoshino Y, Nosaka Y, Nishioka J, Hooker SB, Hirawake T (2021) Diatoms contributing to new production in surface waters of the northern Bering and Chukchi Seas during summer with reference to water column stratification. Prog Oceanogr 199:102692
Tsukazaki C, Ishii KI, Matsuno K, Yamaguchi A, Imai I (2018) Distribution of viable resting stage cells of diatoms in sediments and water columns of the Chukchi Sea, Arctic Ocean. Phycologia 57:440–452
Ueno H, Komatsu M, Ji Z, Dobashi R and others (2020) Stratification in the northern Bering Sea in early summer of 2017 and 2018. Deep Sea Res II 181-182:104820
Yamamoto-Kawai M, Tanaka N, Pivovarov S (2005) Freshwater and brine behaviors in the Arctic Ocean deduced from historical data of $\delta^{18}O$ and alkalinity (1929–2002 A.D.). J Geophys Res Oceans 110:C10003
Yokoi N, Matsuno K, Ichinomiya M, Yamaguchi A and others (2016) Short-term changes in a microplankton community in the Chukchi Sea during autumn: consequences of a strong wind event. Biogeosciences 13:913–923
Zhuang Y, Jin H, Li H, Chen J and others (2016) Pacific inflow control on phytoplankton community in the Eastern Chukchi Shelf during summer. Cont Shelf Res 129: 23–32

Editorial responsibility: Katherine Richardson, Copenhagen, Denmark
Reviewed by: 2 anonymous referees

Submitted: March 29, 2024
Accepted: November 11, 2024
Proofs received from author(s): December 19, 2024